AWARD NUMBER: W81XWH-12-C-0043

TITLE: Ultraviolet Communication for Medical Applications

PRINCIPAL INVESTIGATOR: Lee W. Cross, Ph.D.
Directed Energy, Inc.

CONTRACTING ORGANIZATION: Directed Energy, Inc. (DEI)
Lexington, KY 40511-1267

REPORT DATE: May 2014

TYPE OF REPORT: Annual

PREPARED FOR: U.S. Army Medical Research and Materiel Command
Fort Detrick, Maryland 21702-5012

REPORT DOCUMENTATION PAGE

Form Approved
OMB No. 0704-0188

1. REPORT DATE	2. REPORT TYPE	3. DATES COVERED *(From - To)*
May 2014	Annual	1 MAY 2013 to 30 APRIL 2014

4. TITLE AND SUBTITLE

Ultraviolet Communication for Medical Applications

5a. CONTRACT NUMBER
W81XWH-12-C-0043

5b. GRANT NUMBER
W81XWH-12-C-0043

5c. PROGRAM ELEMENT NUMBER

5d. PROJECT NUMBER

6. AUTHOR(S)

Lee W. Cross
Mohammad J. Almalkawi

5e. TASK NUMBER

5f. WORK UNIT NUMBER

7. PERFORMING ORGANIZATION NAME(S) AND ADDRESS(ES)

Directed Energy, Inc. (DEI)
1500 Bull Lea Rd STE 212
Lexington, KY 40511-1267

8. PERFORMING ORGANIZATION REPORT NUMBER

9. SPONSORING / MONITORING AGENCY NAME(S) AND ADDRESS(ES)

U.S. Army Medical Research and Materiel Command (USAMRMC)
Fort Detrick, MD 21702-5012

10. SPONSOR/MONITOR'S ACRONYM(S)
USAMRMC

11. SPONSOR/MONITOR'S REPORT NUMBER(S)

12. DISTRIBUTION / AVAILABILITY STATEMENT

DISTRIBUTION A: Approved for Public Release; Distribution Unlimited

13. SUPPLEMENTARY NOTES

Report contains color.

14. ABSTRACT

Under this Phase II SBIR effort, Directed Energy Inc.'s (DEI) proprietary ultraviolet (UV) emitters and the best available electro-optic components are employed to implement a functional prototype demonstrating short range, medium data rate non-line-of-sight (NLOS) optical communication data links operating in the solar blind region (200–280 nm). The intended application is covert wireless transfer of medical data for battlefield combat casualty care. During the course of this effort and after detailed investigation pertinent to this technology through simulation, system studies, field trials, and review of current and future technologies, hardware components were designed and integrated into a functional breadboard system demonstrating: (1) unidirectional communication of medical data in outdoors environment; and (2) bidirectional communication of medical data with encryption and forward error correction. Work in the second half of the Phase II project will extend the test bench implementation to be capable of mobile ad-hoc networking, and will repackage the system as a brassboard module suitable for field trials.

15. SUBJECT TERMS

Non-line-of-sight (NLOS), networking, optical communication, plasma-shells, short range, ultraviolet (UV) light

16. SECURITY CLASSIFICATION OF:			17. LIMITATION OF ABSTRACT	18. NUMBER OF PAGES	19a. NAME OF RESPONSIBLE PERSON
a. REPORT	b. ABSTRACT	c. THIS PAGE			Dr. Gary Gilbert
Unclassified	Unclassified	Unclassified	UU	16	19b. TELEPHONE NUMBER *(include area code)* 301-619-4043

Table of Contents

Introduction

This project investigates the efficacy of short range (up to 50 m), medium data rate (at least 57.6 kbps) non-line-of-sight (NLOS) optical data communication using ultraviolet (UV) light in the solar blind region (200–280 nm wavelength). The application is wireless transfer of medical data for battlefield combat casualty care. The investigated scenario is medical data transfer between a patient-worn vital sign monitor to a medic PDA from the initial site of trauma in outdoor environments with diverse atmospheric conditions to indoor areas including evacuation vehicles and forward combat support hospitals. To date, no researchers have experimentally demonstrated compact transceivers capable of adequate range and data rate. In the previous Phase I effort, Directed Energy Inc.'s (DEI) parent company Imaging Systems Technology (IST) demonstrated feasibility of several key concepts are being developed into a working prototype in the Phase II effort to meet Army requirements for a UV NLOS communication device.

Body

Under this Phase II SBIR, DEI's main objective is to develop prototype UV optical communication hardware to create a flexible hardware platform that can be easily integrated into a variety of applications relevant to the Army medical mission. In this context, research progress since the beginning of the Phase II effort (May 2013) to date is outlined in this section.

Task 1. Simulation

Monte Carlo photon scattering simulation requires considerable processing power to accurately model high path loss. A high-end simulation computer was identified as a critical need and ordered in Phase II. Simulation will be done using a GPU-assisted processing library known as CUDA. The massively parallel CUDA architecture is ideal for achieving many orders of magnitude speed-up in Monte Carlo photon scatter simulations, which allows better exploration of the design space, but prior to using this approach CPU processing was first investigated. Monte Carlo code written in Phase I was run on two computers: a desktop computer with an Intel i5 3.4 GHz quad-core processor, and the new server with dual Intel Xeon 3.1 GHz processors (16 cores total). The simulated pulse contained 270 billion photons. The quad-core desktop computer simulated 1.16 million photons per second per core, requiring 16.2 hours for one pulse. The Xeon server with slightly lower clock speed simulated 1.07 million photons per second per

core. Xeon processors use Hyper-Threading and are therefore capable of executing twice as many simulation threads, so with 32 threads one pulse was simulated in 2.2 hours for a speed-up of 7.4X. CUDA is expected to be another order of magnitude speed-up by increasing raw processing power from 397 GFLOPs (CPU) to 4500 GFLOPs (GPU). Further benefit of using multiple GPUs can be assessed for free using Microway's CUDA benchmarking program using multiple high-end GPUs (NVIDIA Tesla K20). Finally, the Monte Carlo simulation task will be resumed after the Milestone 2 demonstration.

Task 2. Plasma-shell Improvement

It was demonstrated in the Phase I Option that our novel three-electrode Plasma-shell pattern shown in Figure 1 will provide the following benefits: higher UVC emission per component, higher drive efficiency, high-speed addressability of the entire Plasma-shell array, and scalable array power emission. This directly supports performance objectives of longer communication range and reduced power consumption.

Figure 1. Plasma-shell with three-electrode pattern.

The Phase II effort began with measuring the Plasma-shell process variation in order to specify tooling and shell handling equipment for the three-electrode system because the new pattern cannot be printed in the same way as the conventional two-electrode pattern. Nominal shell dimensions were 4.40 mm × 2.25 mm (W × H) with ± 0.04 mm tolerance as measured from hundreds of shells, and this is acceptable for automated printing and handling. Next, the option of having our shells electroded by an external company was investigated and DEI accordingly contracted Microtech of Japan, a specialist in handling and applying electrodes to surface-mount components, to investigate the feasibility of high-volume electroding (150,000 Plasma-shells per day). A trial run of 1800 non-lighting shells demonstrated very good electrode quality, and Microtech provided positive feedback about the manufacturability of the machine-printed electrode pattern. A subsequent trial was conducted on lighting shells that were then populated onto an experimental driver board shown in Figure 2(a) that was designed to test different drive and layout options for the three-electrode concept. A separate test fixture was also built to measure Plasma-shell drive charge for precise efficiency measurement. Figure 2(b) shows two green Plasma-shells operating at high brightness. The drive waveform was investigated to increase emission power and addressing speed. The addressable Plasma-shell emitter array will control optical power emission by selecting the number of Plasma-shells to sustain and adjusting drive waveform parameters.

During these experiments two plasma discharge operating modes were observed–a high-efficiency/high-brightness mode and a low-efficiency/low-brightness mode. A sustaining Plasma-shell can transition between these states under different drive conditions, and a series of experiments showed that the transition is affected by changes in drive voltage, drive frequency, and electrode geometry. It was concluded that high-efficiency mode can be stable at moderate drive voltage and frequency, and this operating point coincides with maximum emitted power. However, it was found that electrode geometry must be carefully controlled to enable operation in the preferred mode. To this end, a novel three-electrode drive scheme was experimentally tested so that Plasma-shells operate in high-

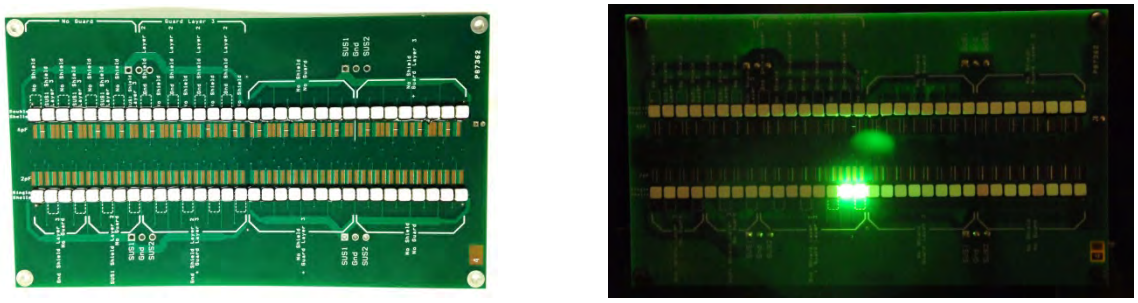

(a) (b)

Figure 2. Fully populated three-electrode Plasma-shell test board: (a) off state; and (b) on-state emission of two addressed Plasma-shells with green phosphor.

brightness, high-efficiency mode with full addressability. The scheme required 3-D electrode patterns with a printed resistive layer and, if the scheme proves to be manufacturable, a small-area emitter module will be designed to demonstrate proof of concept.

In an IR&D effort, the novel three-electrode drive scheme developed for this application was investigated for large-scale manufacturability. Figure 3 shows the prototype 2-inch cube that houses drive electronics and a three-electrode Plasma-shell array that emits UVA light at 350 nm wavelength. These shells were hand-painted with the required conductive and resistive inks. Drive electronics sustain shells with a 940 V square wave at 85 kHz, and shells operate in the high-efficiency discharge mode that produces 3.8 mW per shell. Refinement of the drive electronics and shell electrode geometry improved output power from a previous value of 2 mW per shell at 800 V, 120 kHz. While the UVA output power reported here is much higher than results achieved with UVC shells, improvements here will directly benefit UVC emitter arrays.

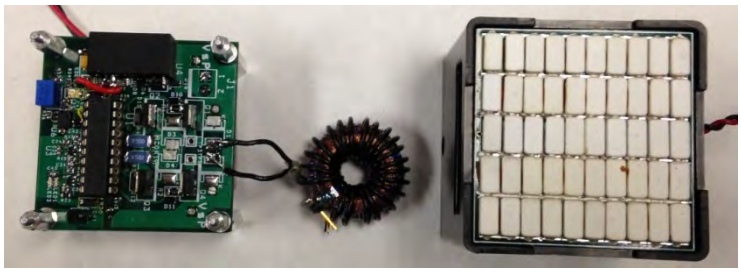

Figure 3. Prototype of a three-electrode panel and drive electronics that fits within a 2 inch cube.

During the last IPR meeting, three questions pertinent to plasma UVC sources were asked. The questions were: what UVC wavelengths are possible, what is the maximum achievable data rate utilizing phosphor down conversion, and what is the maximum achievable UVC production efficiency. In response to the first question, DEI procured several UVC phosphors and tested them with vacuum UV (VUV) excitation. Available emission peaks include: 226 nm, 230 nm, 234 nm, 242 nm, and dual peaks of 253 and 273 nm. All phosphors had similar decay time constants of ~10 μs. Phosphor emission wavelengths and speed are suitable for medium data rate communication in wavelengths shorter than the best available UV LEDs. Finally, it is conceivable that Plasma-shell efficiency can surpass 25% based on the following reasoning. As an initial data point, current red-phosphor-based (680 nm) Plasma-shells operate at 4% radiometric efficiency. A candidate UVC phosphor down converts 90% of 172 nm xenon-emission photons to 241 nm. Down conversion to the shorter wavelength corresponds to 2.9× higher efficiency, and a more

transmissive shell window corresponds to 2× greater output. Further efficiency improvement is possible by increasing the discharge length (by increasing shell length), and changing the gas mixture from a 10% xenon mixture to high-efficiency 30% xenon balance helium mixture. It will be challenging for LEDs to attain this level of efficiency at short wavelengths. The use of shorter wavelengths may significantly benefit UV NLOS applications because of smaller solar blind filters, reduced skin/eye sensitivity, and reduced path loss.

Task 3. Transceiver Hardware

The breadboard system architecture must be flexible to allow easy implementation of a variety of algorithms required in a practical communication system. Therefore, MATLAB was selected as the top-level programming language for this task. Using its Communications System Toolbox, many auxiliary algorithms required by optical communications systems are available as function calls such as: forward error correction (FEC) and detection, coding, modulation, and demodulation. MATLAB code is freely available for encryption, and a toolbox is available for the Zephyr Bioharness to capture streams of patient medical data. When algorithms are tested and found acceptable, they can be manually coded in C++ and targeted for the final prototype hardware. This approach allows rapid prototyping and avoids manual implementation of a wide variety of algorithms.

The block diagram in Figure 4 shows the test bench implementation for the unidirectional medium data rate communication link tested in Milestone 1. Test vectors are used in place of real-time patient medical data, and are generated in the MATLAB control program running on a PC. Data enters the top level of the protocol stack where it is packetized, framed, and modulated. Modulated data is sent to an FPGA board over a high-speed USB link for direct transmission using a pulsed, collimated LED source. UVC photons are received using a photomultiplier tube (PMT) and discriminator, and counts are digitized with an FPGA board and sent to the receive PC via USB. The receiver protocol stack is complementary to the transmit side, with the addition of clock recovery, and demodulated data is analyzed for key link statistics such as bit error rate (BER). The test bench uses two touch-screen panels to control test parameters in the field.

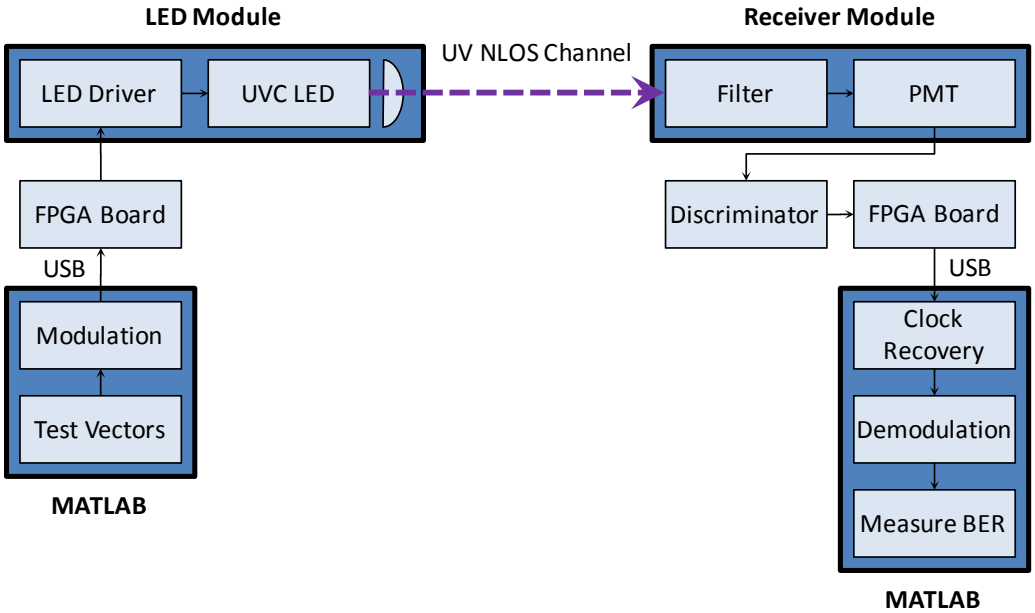

Figure 4. Test bench block diagram for unidirectional data transfer demonstration at 50 kbps, 50 m.

MATLAB communication system code was implemented in a basic, functional way for the first milestone test. Tested data rate was 50 kbps and packet size was fixed to 1024 bits. The modulation scheme was chosen to be 4-PPM, and the slot duty cycle was limited to keep the LED operating at (not beyond) its thermal limit of 1 W_{avg}. Packet boundaries were identified by a fixed sequence of ten leading and ten trailing symbols. On the receive side, discriminator photon count data was sampled at 10 MHz and transmitted to the MATLAB receiver code. Clock recovery was done on the received bit stream using a pattern matching algorithm to identify the fixed packet boundaries. Demodulation was done by calculating the "center of mass" of photon counts within each symbol. Bit error rate (BER) was calculated by comparing the recovered bit stream against the transmitted bit stream. Several MATLAB features were coded but not used in the test bench. First, FEC using low density parity checking (LDPC) codes was implemented but not used because it executed extremely slowly in MATLAB (e.g., decoding one packet in several hours). Faster FEC codes were investigated such as turbo codes for future implementation. Next, channel modeling simulation code was written for an additive white Gaussian noise (AWGN) channel with Poisson arrival statistics, but this simple model has not been used yet.

The successful first milestone test was followed by several investigations on multiple pieces of hardware and firmware in the test bench to improve performance. First, the MATLAB firmware was modified to evaluate the effect of different pulse position modulation (PPM) levels. 2-, 4- and 8-PPM were coded to evaluate the effect on power efficiency. Second, the DEI photon discriminator circuit was simplified to design a multi-channel discriminator for future multi-pixel photon counting sensors. A multi-pixel sensor allows spatial diversity, multiple independent links, and the ability to ignore interference. Third, several FEC algorithms were sought to allow operation at minimum signal-to-noise ratio (SNR) conditions. Coding schemes have been identified that were used in deep-space optical communication links. Fourth, the transmitter and receiver pointing angles were automated with servos to enable automated outdoor channel testing. Finally, DEI purchased and implemented the Zephyr Bioharness MATLAB software development kit (SDK) to import real-time patient medical data into the test bench. Data streams are available for heart rate, breathing, EKG, and physical activity.

Progress on key components of the test bench is reported below:

LED Driver Circuit

To improve LED drive waveforms, an improved pulsed driver circuit was designed and built to achieve faster turn-on/turn-off times by overdriving the LED during transitions. This allows higher modulation speed and more on time during each bit period enabling faster data links to accommodate communication overhead. LED optical emission needs to be observed during rising and falling edges in order to optimize the emission profile, so a silicon carbide (SiC) UV photodiode and amplifier module were constructed.

The communication test bench requires LED emitters that operate at the maximum thermal limit of the UVC LEDs, thus two new LED emitter modules were designed and built that include heat sinks with forced air cooling and integrated pulse driver circuits. The new driver circuit achieves drive current rise and fall time of 100 ns at peak current of up to 10 A.

In relation to the subject matter, DEI participated in a webinar on UVC LED technology hosted by the International Ultraviolet Association (IUVA) on March 2nd, 2014. The webinar brought together industry experts to share their perspectives on the current status and outlook of UVC LEDs and related products. DEI received expert responses on several questions regarding aspects of UVC LED technology related to this application. First, the prospect of developing high-power LEDs with wavelengths shorter than 240 nm appears very likely because there are no direct technology barriers. Second, research-grade UVC LEDs are demonstrating less temperature dependence on output power and lifetime, potentially

enabling long-life operation at higher die temperatures than current generation LEDs that are severely temperature limited. Finally, UVC LEDs are generally capable of good high-current pulsed operation, implying that the premature LED failure experienced in DEI's testing may not reflect a fundamental limitation of UVC LEDs. The expert opinions on these three questions show that UVC LED technology is advancing and may resolve key concerns of this application within the next five years.

Photon Counting Devices

DEI has been working with Hamamatsu and Photonis to investigate and acquire samples of planar photon counting devices such as the Hamamatsu micro-PMT, Photonis Planacon, and Photonis hybrid photodiode. We started with the Hamamatsu C9744 photon counting discriminator module that was reverse engineered so that a reduced-footprint circuit can built into future hardware designs. The Hamamatsu unit also has a noise susceptibility problem that was corrected in DEI's design. Two photon discriminator circuits were designed in-house. The first design intended to duplicate the functionality of the Hamamatsu C9744 discriminator and eliminate its noise sensitivity problem. The second design was a bandwidth-limited trans-impedance amplifier whose output is digitized by a 12-bit analog-to-digital converter (ADC). DEI completed testing of an in-house photon discriminator circuit that achieves identical performance as the C9744 discriminator, and resolves the false-triggering problem. The design will be useful with multi-pixel photon counting sensors.

A related question was asked about the photon counting sensor during the IPR meeting. It was pointed out that if a large-area sensor were used as DEI proposed, the dark count would become a critical performance parameter and could negate any benefit of larger area. The current sensor is a Hamamatsu R7154 PMT, and average dark count is ~600 counts per second (CPS) with active area of 1.9 cm^2. The proposed use of a large-area sensor such as the Photonis hybrid photodiode (HPD) would yield significant improvement; average dark count is only ~25 CPS with larger area of 4.9 cm^2 when using a Cs-Te solar blind photocathode material. It is hoped that the ADC approach will work with the PMT in both photon-counting and linear modes for operation over a high dynamic range, which will improve performance in light-saturated conditions such as during jamming.

UVC Filter

The PMT enclosure shown in Figure 5 was designed and built to protect the water-soluble UVC filter from humidity by sealing the PMT, UVC filter measuring 25 mm diameter × 15 mm thick, and desiccant pack in an air-tight compartment. The enclosure has mounting points for the PMT base, a laser sight for alignment, an iris to cover the filter, and a ¼"-20 threaded hole for tripod mounting. The assembly is completed utilizing the Schott UG5 black glass filter that blocks the visible passband of the UVC filter and is chemically stable for use as the outer window material. The UVC filter is a proprietary nickel sulfate ($NiSO_4$) material called UVC7 from INRAD Optics that is more stable across temperature and humidity exposure than pure nickel sulfate.

Spectral responses of three UVC filter stackups shown in in Figure 6 were measured with respect to the emission of a UVC Plasma-shell (e.g., the black reference line). Spectra provide limited information because they are near the noise floor of the spectrometer, and total light collection was affected by filter thickness, refractive index, and sidewall reflectivity. Despite this, it can be seen that the UVC7 filter passes the two UVC peaks and blocks everything except a wide passband around blue (e.g., ~500 nm). The two black glass filters attempt to block the blue band and the UV11 material is far more effective than the UV5 material. It is likely that an organic filter material will be needed to provide additional attenuation at 300–350 nm. Further testing is needed to measure the combined response of the photon counting receiver module with filters.

Figure 5. The custom air-tight PMT housing on the left protects the water-soluble UVC filter on the right.

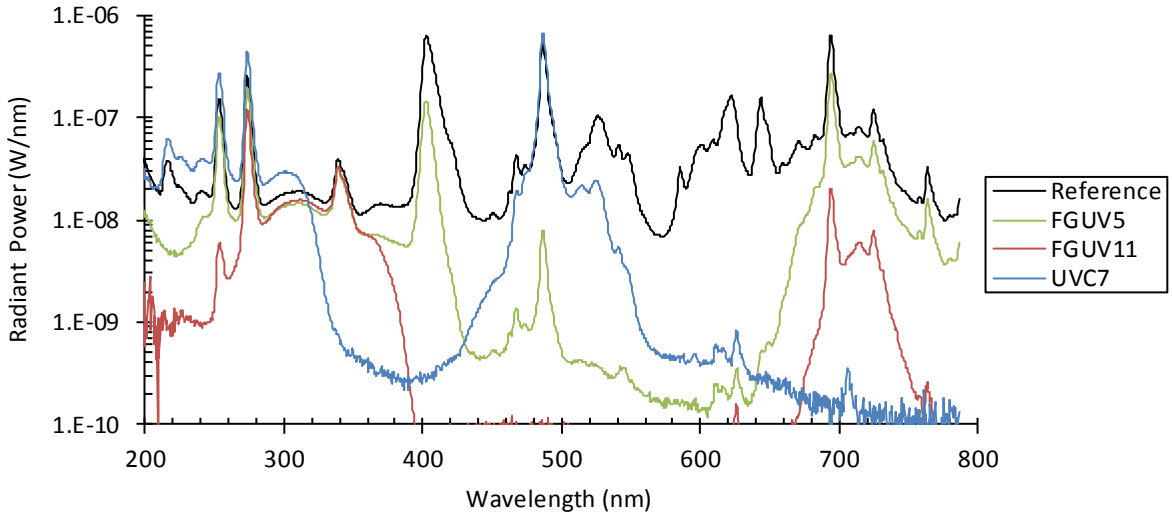

Figure 6. Spectra of UVC Plasma-shell light emission (e.g., reference line) through three filters: Schott UV5 (FGUV5), Schott UV11 (FGUV11), and INRAD UVC7. Multiple filters must be stacked to achieve an acceptable solar blind sensor response.

Next, the solar blind filter was investigated to determine if it is possible to reduce the physical size. To this end, the concept of using shorter-wavelength UV radiation is being considered. Based on the solar irradiance spectrum at the surface of the earth, it is known that wavelengths shorter than 280 nm do not contribute significant background photon counts. The use of short-wavelength UVC LEDs or Plasma-shells may allow a solar blind filter stackup with slower roll-off around 280 nm. This could enable the use of organic filter materials (rather than thick doped crystalline materials) to achieve high rejection without requiring a sharp rejection skirt. Available UVC filters do not have sufficient UVA and visible wavelength rejection to operate in direct sunlight–this will require an additional organic filter material custom tailored for this application. The current filters do, however, have sufficient performance to block the much weaker natural and artificial light sources at night, so outdoor testing was conducted within the city of Toledo to measure filter performance in the presence of street lights, star light, and general night-time light pollution. The result was that the worst-case background photon count rate was 0.014 counts per μs when using the UVC7 and FGUV5 filters together. This corresponds to 0.13 counts per modulation slot period at the unidirectional data rate of 50 kbps. The Milestone 1 test had a favorable signal-to-noise ratio with this configuration when tested at night. This line of investigation will be ongoing.

Task 4. Network Protocol

In this task, networking protocols were investigated to support the project objective of seamlessly integrating UVC communication nodes into complex multi-hop network architectures. At this point it is

assumed that a conventional Ethernet network using TCP/IP protocol should provide a suitable development environment for early work. We are defining hardware and functional requirements to interface an optical communication module with an Ethernet network and their compatibility with existing networking technologies. The goal of this task is to achieve the ability to interface with standard internet protocol (IP) network hardware and route IP packets through the optical network. The Department of Defense (DoD) extensively uses internet protocol (IP) networks, so this is a logical protocol to target for compatibility. A description of the intended networking approach is listed below.

The optical network should support protocols including transport control protocol (TCP) and user datagram protocol (UDP), and this will allow a wide variety of services to be operated over the optical network including FTP, HTTP, SMTP, DNS, streaming audio and video, etc. The optical network topology will be multi-hop ad-hoc, so routing becomes a key issue. The optical network will be responsible for routing IP traffic between optical nodes and gateways. Therefore, each optical node will require the basic ability to route traffic across the optical network. A simple and robust approach for mobile networks is dynamic source routing, whereby each node that originates data (e.g., a transmitting node or a gateway passing data from the wired network) is responsible for identifying and maintaining the routing path over the optical network. A media access control (MAC) layer must also be defined for the optical network to control access to the shared communication medium (the optical propagation path). The MACAW protocol is often used by mobile networks to allocate communication time slots and resolve packet collisions. These networking concepts will be integrated into the test bench hardware starting with the lowest layer (MAC layer). Each layer will be successively added to build out full networking functionality.

Figure 7 shows a flexible architecture that can readily support UV NLOS networking and bridging to other IP networks. In this conceptual network adapter, functionality is implemented in software and

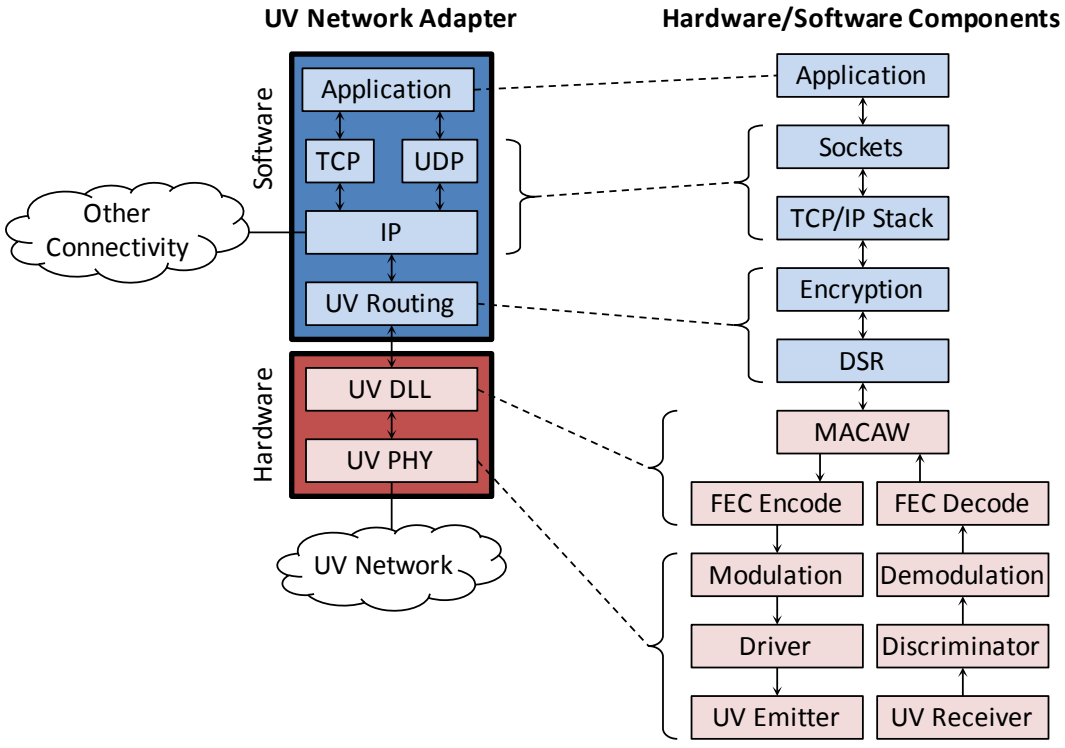

Figure 7. UV network adapter partitioning between hardware and software, supporting all necessary functions and protocols to route data across UV NLOS and conventional IP networks.

hardware to provide a balance of performance and flexibility. For stand-alone applications, the adapter may include a custom application and support for network sockets. For all applications, the adapter supports software-based UV-NLOS-specific routing protocols (and per-packet encryption) and hardware dynamic link layer (DLL) and physical layer (PHY) functions. The DLL includes logical link layer (LLL) functions such as forward error correction (FEC) and packet framing, and media access control (MAC) protocols to arbitrate the half-duplex optical communication medium. At the lowest level, the module includes UV emitter and receiver devices with associated circuitry, and implements modulation and demodulation.

The next concept to introduce is network bridging, where IP traffic can seamlessly cross from the UV mesh network to a conventional wired network. This requires functionality that determines if IP packets should cross the boundary, and implements DSR for packets that enter the UV network. A network bridge serves as a network access point to connect the UV network to IP networks and internetworks. Data flow is visualized through a network bridge in Figure 8.

Another concept to consider in this task is connecting an IP source to a network adapter across a serial link as shown in Figure 9. This comes into play in the proposed work when network access needs to be

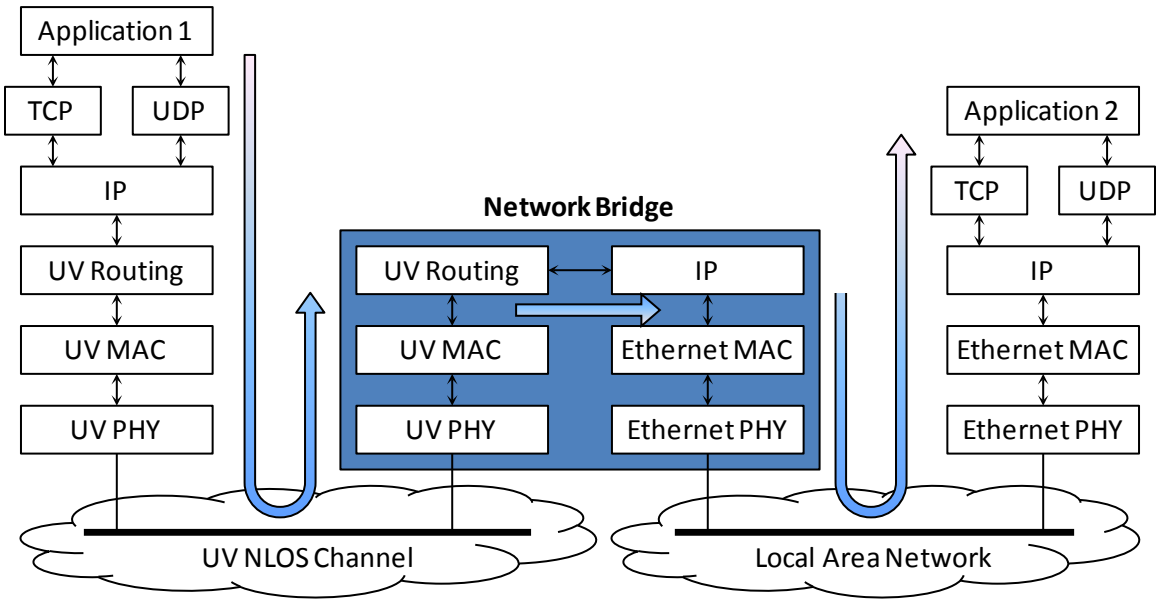

Figure 8. Network bridging joins a UV network with a conventional LAN.

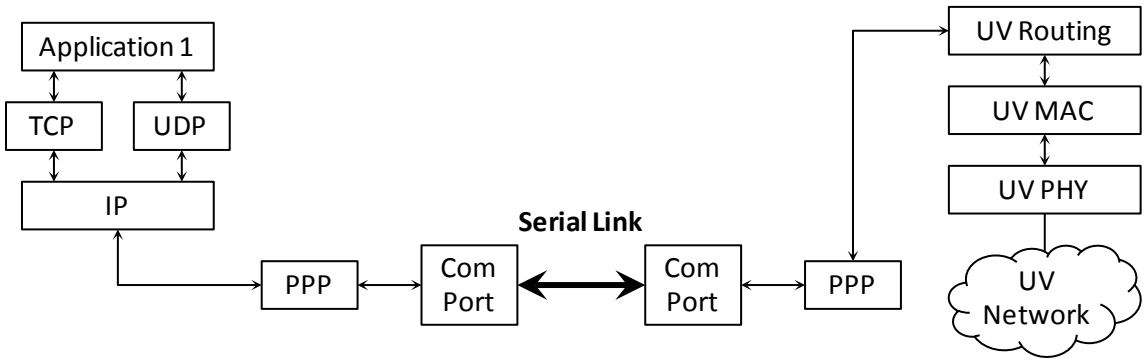

Figure 9. PPP connects an application to the UV network across a serial link.

provided over a serial link such as USB or RS-232. IP packets can be transmitted across serial links using the general-purpose point-to-point protocol (PPP) or the simpler serial line internet protocol (SLIP). This concept can be used with handheld PDAs and serial connections to the UV network access point.

Further network protocol planning will be resumed after the bidirectional milestone is completed.

Task 5. Testing

Milestone 1 - Unidirectional Communication

The test bench hardware and software block diagram was mentioned previously in Figure 4. Data flows in the clockwise direction, originating as a random number test vector on the left and being recovered and analyzed on the right. The test bench implements a basic data link operating at 50 kbps and measures noise counts (received photons and dark counts with the transmit LED off), combined average signal and noise counts, and received BER. Calculated SNR and BER for many bits (10^5 in this test) are basic measures of link performance.

Measured SNR at three ranges is shown in Figure 10. The elevation angle of the transmit LED is indicated in the legend, as either pointed slightly over the receiver (10°) or aimed somewhat higher (30°). Average transmit power is doubled by using two LEDs, where each LED module transmits approximately 7 mW average optical power into the atmosphere. The PMT receiver is pointed at an elevation angle of 45° and is filtered by the UVC7 and black glass filters. The test was conducted at night because the current filter stackup is insufficient to fully reject daylight. With this test setup, BER was measured to be 0 for all points except those circled, where SNR was sufficiently low to experience errors. It can be seen that the system requires a SNR of at least ~9 dB to operate, and this can be reduced to closer to 1–2 dB using improved coding. This would enable a significant reduction in transmitted power.

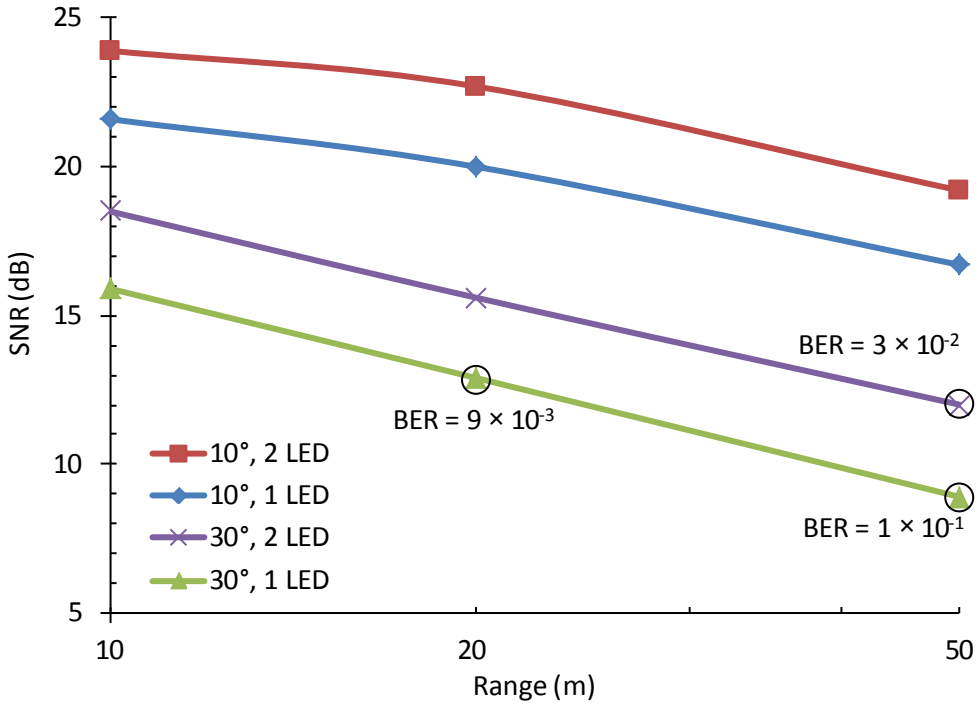

Figure 10. Milestone 1 test data showing SNR versus range with BER.

The test bench software was updated to implement AES-128 encryption on payload packets. The AES cipher is NSA approved for classified information: 128-bit key length is sufficient for SECRET level, and 192- and 256-bit key lengths can be used for TOP SECRET information.

After Milestone 1 testing was completed, the hardware test bench was tested with two additional functions: real-time data transfer of medical data, and encryption. The test bench diagram in Figure 11 shows the hardware and software configuration several months after Milestone 1 testing. Real-time patient vital sign data is imported from a Zephyr Bioharness into MATLAB where patient data is packetized and encrypted. Packets are framed and modulated prior to transmission by the FPGA board. The reverse process is applied at the receiver and the real-time medical data stream is presented on a dashboard graphical interface.

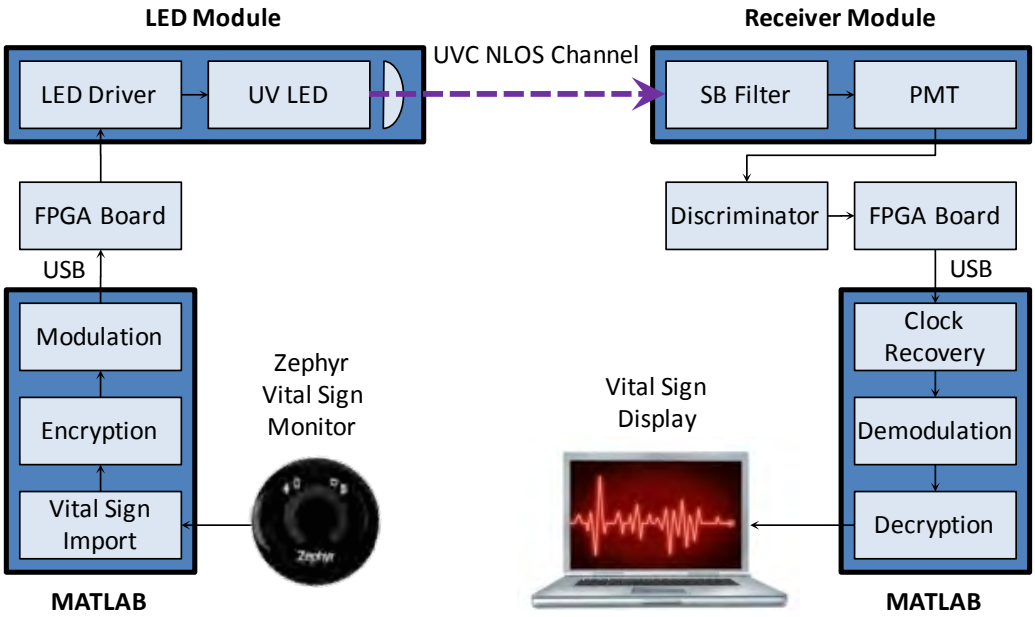

Figure 11. Test bench configuration for real-time transfer of secure (encrypted) medical data from a Zephyr Bioharness for display on a remote laptop.

Milestone 2 - Bidirectional Communication

The goal of the next series of tests will be to improve power efficiency (i.e., reduce transmitted optical power). Two tests will be conducted: vary modulation levels, and use turbo codes. Different PPM and demodulation levels were developed in MATLAB code. This includes 2, 4, and 8 levels per symbol to investigate the trade-off between bandwidth and power efficiency at a given BER. Turbo convolutional codes, a class of high-performance FEC codes, are also under development for the test bench. The principle of operation is encoding interleaved redundant data streams and then decoding at the receiver side using two decoders that work on different code words. Decoders share information in order to improve the probability of converging on the correct solution, and the iterative algorithm improves the level of convergence based on the number of iterations. Turbo codes perform best for low code rate and moderate data rate applications, and have the following advantages: burst error correction; performance approaching Shannon's capacity limit; and remarkable power efficiency for moderately low BER. Turbo codes are used in modern 3G communication networks (i.e., suitable for delivery of multimedia services) and deep-space communication. One drawback of turbo codes is high latency/delay due to interleaving and iterative decoding. Design tradeoffs will be investigated to

determine the resulting BER under various scenarios such as: number of iterations; channel conditions; packet size; number of parity bits, etc.

To achieve a higher error correction capability, Turbo convolutional codes have been developed and are currently being integrated into the test bench. Turbo codes work in an iterative fashion to achieve the optimal level of convergence. During the development stage, several iteration amounts have been tested and it was observed that 10 iterations are sufficient for minimum BER. In the developed Turbo codes, two Recursive Systematic Convolution (RSC) encoders and two iterative Bahl Cocke Jelinek Raviv (BCJR) decoders were used. The two RSC encoders are in a parallel concatenation to allow simpler decoding and separated by an interleaver. The two encoders are identical and the code is systematic. The function of the interleaver is to randomize the input information bits and provide them to the second encoder, while the first encoder receives the data as it is with no interleaving. The choice of interleaver is crucial in order to ensure diverse encoder outputs that will result in better decoding performance. A pseudo-random interleaver is used by generating pseudo-random integers from 1 to the length of the information message, and then the message is interleaved based on the generated sequence. Our selection to the interleaver type is based on several literature articles stating that pseudo-random interleavers outperform other interleaving methods for larger block sizes. A code rate of 1/3 is used and consists of the original (systematic) information data and the outputs of the 1^{st} and 2^{nd} encoders. At the receiver side, the Turbo decoder (comprised of two decoders) determines the log likelihood ration (LLR) to estimate the binary bit received; hence, soft decision is used. This allows operation closer to the maximum theoretical power efficiency.

In order to streamline link testing, a generalized MATLAB GUI was implemented to allow on-the-fly communication configuration changes including: selectable number of packets, modulation type (i.e., modulation levels of m-ary PPM), LED duty cycle, and LED current. Vital sign data is graphically displayed along with link statistics such as BER, signal strength, and photon counts.

The test bench software is ready to test power efficiency with respect to modulation depth and forward error correction (FEC), however initial tests of large data sets showed stability and nonlinearity problems with the hardware. The problem was isolated to the UVC LED and driver circuit, and a new PCB layout is being made to correct the problem.

Also in preparation for the second milestone demonstration of bidirectional communication, two complete sets of send/receive hardware were built. Hardware modules are being integrated into a fully bidirectional system, and the MATLAB control program was modified to enable bidirectional operation. Several components were tested including Gefen USB extenders to use 50 m USB cable runs, and the DEI photon discriminator design was validated and found to be 10% more sensitive than the Hamamatsu unit. A new motor controller board has been designed to automate the pointing angles of the transmitter and receiver assemblies. The emitter positioner driver board is now operational and a second positioning stage is being built to allow automated measurement of path loss versus sender and receiver elevation. A solar blind hybrid photodiode (HPD) from Photonis with a passband at 260 nm was ordered, and the larger area and reduced profile will benefit the planned brassboard system.

One Crystal IS UVC LED was destructively tested to measure its ability to handle high-current, short-duration pulses. This is beneficial for accomplishing higher-level pulse position modulation (PPM) in order to achieve better power efficiency. The LED was tested with low duty cycle pulses from 1000 mA peak current up to 5000 mA. The LED die was permanently damaged by high peak current at 1500 mA, however, rapid aging was observed even at the lowest drive level of 1000 mA. This latest-generation device could not withstand high peak currents and should therefore be operated below 1000 mA; however industry experts have indicated that this premature failure is not typical of all UVC LEDs operated at high pulsed current. Further testing is needed to determine the aging effect at lower drive

currents. It was also observed that light emission decreased by 32% when ambient temperature increased by 32 °C. This implies that current UVC LEDs must be effectively cooled to maintain emitter efficiency.

The bidirectional test bench hardware and firmware is being integrated to demonstrate bidirectional communication for the Milestone 2 demonstration. Milestone 2 testing will coincide with the end of the first year, so results will not be available until the next monthly reporting period.

Ongoing Plasma-shell Aging Data

Aging data for UVC Plasma-shells manufactured at the start of Phase I is shown in Figure 12 where average power for three shells is normalized to burn-in time of 24 hours. Output power at the most recent sampling time of 15,840 hours is 79% of initial power at 24 hours. This demonstrates that Plasma-shells have superior lifetime compared to UVC LEDs with lifetimes as short as 1000 hours.

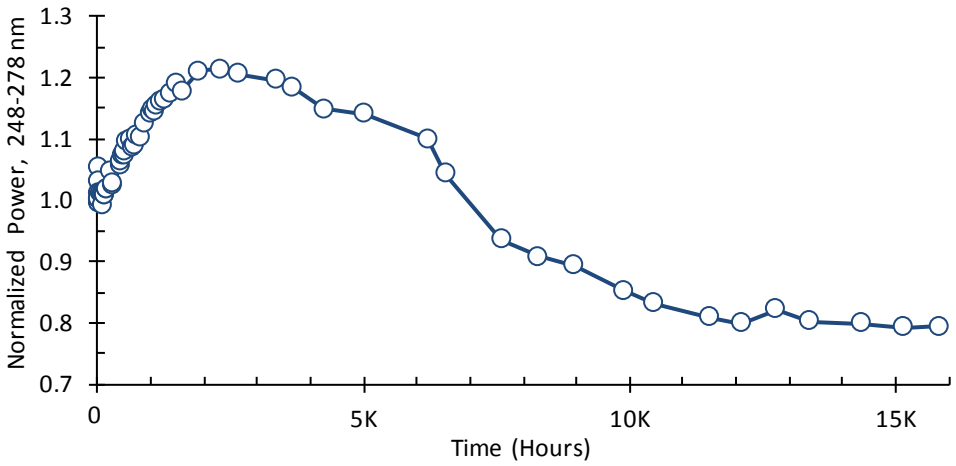

Figure 12. Plasma-shell UVC power at 15,840 hours is 79% of initial value.

Key Research Accomplishments

- Milestone 1 successfully demonstrated a unidirectional medium data rate communication link.
- Hardware and firmware for Milestone 2 demonstrating a bidirectional communication link is being integrated. Results will be reported in the next monthly report.
    - Two sets of send/receive hardware were built and integrated into the test bench.
    - MATLAB control program was modified for time-multiplexed bidirectional operation.
    - Test bench is fully automated for communication parameters and pointing angles.
- UVC-emitting Plasma-shell
    - Demonstrated lifetime exceeding 15,840 hours (and counting).
    - Manufactured 3-electrode Plasma-shell array packaged within a 2-inch cube enclosure
    - A pathway to short-wavelength (< 240 nm), high-efficiency (> 25%) Plasma-shell emitters was identified.
- Established relationships with key suppliers and interested parties
    - Microtech, for high-volume electroding of Plasma-shells
    - UVC component manufacturers: Photonis, Hamamatsu, Crystal IS
    - Potential applications: Robotics Research LLC, Think-a-Move Ltd., and Engility Corp.
- Proposed networking protocols compatible with existing networking technologies

- MATLAB GUI was implemented to allow on-the-fly communication configuration of: selectable number of packets; modulation type; LED duty cycle and LED current; vital sign statistics; and link statistics such as BER, signal strength, and photon counts.

Reportable Outcomes

- The state of Kentucky awarded $500,000 of matching funds under Grant Agreement KSTC-184-512-13-167 to develop and commercialize this technology. As a result, the Phase II contract was novated to the newly created Kentucky-based subsidiary company DEI that was formed to develop and commercialize this technology.
- DEI hired Dr. Almalkawi as full-time researcher for this project. His background in communication systems will benefit all aspects of this project.
- DEI attended the SOCOM Tactical Assault Light Operator (TALOS) industry collaboration event at MacDill AFB November 19-20, 2013. UVC NLOS communication was proposed as a method for covert data communication integrated into a battle suit. There was interest in NLOS technology for security products and UAV command and control.
- DEI attended the C4ISR medical exercises on July 23, 2014 at Fort Dix. Observations of medical exercises and interviews of program officers and enlisted personnel have been beneficial for understanding intended use cases for this technology.
- Submitted two Phase I SBIR proposals for related UV NLOS communication applications.
- Submitted two Phase II SBIR proposals for synergistic Plasma-shell research to accomplish UVA and UVC water purification and photocatalytic microbial deactivation.
    - Synergistic benefits of completed Phase I contracts include: improved shell transparency by 20%, and increased UVA emission.
- Recent commercialization activities of synergistic UV Plasma-shell technology:
    - Contracted by Aquionics to produce UVA Plasma-shell modules for UV sterilization.
    - Contracted by EPA to produce UV Plasma-shell water purification modules.

Summary and Conclusion

The UV spectrum is currently unused and is not susceptible to RF interference, jamming, or microwave attack. This presents opportunities for achieving covert communication especially in situations requiring radio silence. Potential applications beyond combat casualty care include: voice communication within fire teams and squads; unmanned aerial/ground vehicle (UAV and UGV) operation; convoy networking, and unmanned ground sensor (UGS) networks.

In this report that covers the first year of research and testing, the required networking theory, prototype hardware and firmware of UV NLOS optical communication system was investigated, and a hardware and software test bench was successfully implemented and tested that achieved unidirectional UV NLOS data communication at a range up to 50 m at 50 kbps data rate. After this Milestone 1 testing was completed, DEI improved several test bench components and algorithms to increase efficiency and equivalently reduce power consumption required to drive the LED sources. Hardware and software components of a bidirectional communication test bench were integrated for the bidirectional Milestone 2 test. This will be followed by the incremental addition of test bench capability to achieve the full set of performance goals laid out in the solicitation topic, resulting in a field-tested brassboard device in the project's second year.